remote sensing

MDPI

Article

TCCON Philippines: First Measurement Results, Satellite Data and Model Comparisons in Southeast Asia

Voltaire A. Velazco [1,*,†] Isamu Morino [2], Osamu Uchino [2], Akihiro Hori [2], Matthäus Kiel [3], Beata Bukosa [1], Nicholas M. Deutscher [1], Tetsu Sakai [4], Tomohiro Nagai [4], Gerry Bagtasa [5], Toshiharu Izumi [4], Yukio Yoshida [2] and David W. T. Griffith [1]

1 Centre for Atmospheric Chemistry, School of Chemistry, University of Wollongong, Northfields Ave., Wollongong, NSW 2522, Australia; bb907@uowmail.edu.au (B.B.); ndeutsch@uow.edu.au (N.M.D.); griffith@uow.edu.au (D.W.T.G.)

2 Satellite Observation Center, National Institute for Environmental Studies (NIES), Onogawa 16-2, Tsukuba, Ibaraki 305-8506, Japan; morino@nies.go.jp (I.M.); uchino.osamu@nies.go.jp (O.U.); hori.akihiro@nies.go.jp (A.H.); yoshida.yukio@nies.go.jp (Y.Y.)

3 California Institute of Technology, Pasadena, CA 91125, USA; mkiel@caltech.edu

4 Meteorological Research Institute, 1-1 Nagamine, Tsukuba, Ibaraki 305-0052, Japan; tetsu@mri-jma.go.jp (T.S.); tnagai@mri-jma.go.jp (T.N.); toshiharu-izumi@met.kishou.go.jp (T.I.)

5 Institute of Environmental Science and Meteorology, University of the Philippines Diliman, Quezon City 1101, Philippines; gerrybagtasa@gmail.com

* Correspondence: voltaire@uow.edu.au; Tel.: +61-2-4221-5527

† Also Fellow at: Oscar M. Lopez Center for Climate Change Adaptation and Disaster Risk Management Foundation, Inc., Philippines

Received: 8 September 2017; Accepted: 22 November 2017; Published: 28 November 2017

Abstract: The Total Carbon Column Observing Network (TCCON) is a global network dedicated to the precise and accurate measurements of greenhouse gases (GHG) in the atmosphere. The TCCON station in Burgos, Ilocos Norte, Philippines was established with the primary purpose of validating the upcoming Greenhouse gases Observing SATellite-2 (GOSAT-2) mission and in general, to respond to the need for reliable ground-based validation data for satellite GHG observations in the region. Here, we present the first 4 months of data from the new TCCON site in Burgos, initial comparisons with satellite measurements of CO_2 and model simulations of CO. A nearest sounding from Japan's GOSAT as well as target mode observations from NASA's Orbiting Carbon Observatory 2 (OCO-2) showed very good consistency in the retrieved column-averaged dry air mole fractions of CO_2, yielding TCCON - satellite differences of 0.86 $\pm$ 1.06 ppm for GOSAT and 0.83 $\pm$ 1.22 ppm for OCO-2. We also show measurements of enhanced CO, probably from East Asia. GEOS-Chem model simulations were used to study the observed CO variability. However, despite the model capturing the pattern of the CO variability, there is an obvious underestimation in the CO magnitude in the model. We conclude that more measurements and modeling are necessary to adequately sample the variability over different seasons and to determine the suitability of current inventories.

Keywords: greenhouse gases; remote sensing; TCCON; tropical western Pacific; Asian pollution outflow; GEOS-Chem; Mie and Raman LiDAR; megacity emissions

1. Introduction

The United Nations Climate Change Conference, COP21, held in Paris in 2015, resulted in countries agreeing on a common goal: to mitigate global warming. In the Paris Agreement, each country is given freedom to determine, plan and regularly report its own contribution to these

mitigation efforts. These contributions are called "nationally determined contributions" (NDCs). Despite the fact that each Party's NDC is not legally binding, there is a legal commitment from each Party to have their progress tracked by technical expert review to assess the achievement toward the NDC [1]. Moreover, Article 13 of the agreement highlights an "enhanced transparency framework for action and support" that establishes harmonized monitoring, reporting, and verification (MRV) requirements. Increased levels of the two major greenhouse gases (GHGs), atmospheric carbon dioxide (CO_2) and methane (CH_4), are responsible for man-made global warming. Mitigation of global warming depends on reducing, if not eliminating, the emissions of these gases. It follows that in order to realize the goals of COP21, accurate and precise monitoring of these greenhouse gases is mandatory. Management of emissions requires measurements of emissions.

The Total Carbon Column Observing Network (TCCON) is a ground-based network of measurement stations that employ high-resolution Fourier transform spectrometers (FTS). The network is designed to retrieve precise and accurate column abundances of greenhouse gases such as CO_2, CH_4, H_2O, N_2O and trace gases, such as CO from near-infrared (NIR) solar absorption spectra [2]. TCCON retrieves column-averaged dry air mole fractions (DMFs; denoted X_G for gas G) by normalizing to the retrieved oxygen column. With this method, TCCON achieves a precision of better than 0.25% for CO_2 over the whole network [2]. DMFs are unaffected by variations in atmospheric pressure and atmospheric water vapor. Since TCCON integrates the whole column of gases above the surface, the horizontal gradients of X_G, which would be measured at different TCCON stations, are more directly related to the underlying regional scale fluxes.Because the TCCON data are tied to the World Meteorological Observation (WMO) scale, TCCON serves as the link between the calibrated surface in situ measurements and the satellite measurements.

The new TCCON station in Burgos, Ilocos Norte, Philippines was established to respond to the need for a ground-based station in the Southeast Asian region, with the primary purpose of validating the Greenhouse gases Observing SATellite-2 (GOSAT-2) mission set to be launched in 2018/2019. GOSAT-2 will continue the work of GOSAT, which was launched in 2009 and the first satellite in orbit specifically designed to measure greenhouse gases CO_2 and CH_4 [3,4]. Additionally, this new TCCON station will provide much-needed validation in general to current and future missions (e.g., NASA's Orbiting Carbon Observatory 2 (OCO-2) [5], OCO-3 [6] and Europe's Sentinel-5P [7]) as well as help improve the uncertainty in quantification of greenhouse gas sources and sinks in the Southeast Asian region [8], a region undergoing significant economic and population growth, with energy-related CO_2 emissions projected to double (2.4 Gt) by 2040 [9].

In this work, we show first measurements of greenhouse gases CO_2, CH_4, H_2O and the trace gas CO from the TCCON station in Burgos. We also show results of measurements from a two-wavelength polarization Mie and Raman LiDAR developed for GOSAT-2 validation that is installed inside the same container as the TCCON instrument and is currently the only one of its kind in the Philippines. We further report initial comparisons with satellite retrievals of CO_2 from GOSAT and OCO-2. Section 2 describes the data from these instruments, the backward trajectory analyses and the set-up of the GEOS-Chem model that we used for investigating the CO measured at the site. GOSAT-2 will have the additional capability to measure CO. Combined measurements of CO_2 and CO have been shown to reduce uncertainties in CO_2 flux estimates from simulated satellite observations because CO provides a better signal-to-noise ratio on the combustion sources than the CO_2 measurements alone [10]. In Section 3, we further investigate the satellite data comparisons and the tagged-tracer studies of CO from the GEOS-Chem model. We briefly discuss the results in Section 4, where we also interpret the elevated CO with the help of the model simulations, results from the LiDAR and results from previous studies in the region. Finally, we provide conclusions in Section 5.

2. Materials and Methods

2.1. Site Description

The measurement site is located in Burgos, a town in Ilocos Norte province in the northernmost part of Luzon Island in the Philippines (18.52°N, 120.65°E, see also TCCON stations map at: http://tccondata.org/). The town of Burgos has a small population of about 10,000 people and is approximately 55 km from Laoag City, the capital of Ilocos Norte province. The whole province of Ilocos Norte has been declared a "coal free province", meaning that no coal-fired power generating facilities are allowed to operate in the region. The absence of strong point sources in the vicinity of the TCCON site will allow easier discernment of pollution signals brought about by long-range transport because the site experiences a variety of clean and polluted scenarios, i.e., relatively clean marine air from the western Pacific is sampled but depending on season, polluted air from long range transport reaching the site can be detected. We investigate this with the help of X_{CO} measurements combined with modeling and LiDAR measurements. For more details on the site, its location and characterization, please refer to: https://www.cddjournal.org/article/view/vol02-iss2-1 [11].

2.2. Instrumentation

The main instrumentation consists of a TCCON instrument and a two-wavelength polarization Mie and Raman LiDAR. Auxiliary instruments also provide measurements of meteorological parameters required by a TCCON station. The main instruments are briefly described below.

2.2.1. TCCON FTS

We use a high-resolution (HR) FTS, model Bruker IFS 125 HR (Bruker Optik GmBH, Ettlingen, Germany) with a maximum spectral resolution of 0.0035 cm^{-1}, which is housed inside an air-conditioned, weatherproof container (for details see [11]). The instrumentation, measurement procedures, software, data processing, etc. all follow TCCON protocols as described in [2]. Remote-controlled manual operation (via internet) with on-site support is carried out on most sunny days. Column-averaged DMFs are retrieved using the 2014 version of the TCCON processing software called GGG [12].

2.2.2. LiDAR System for GOSAT-2 Validation

The main purpose of our LiDAR observations is to investigate the influence of atmospheric aerosols and thin cirrus clouds on GOSAT data. We aim to do this based on simultaneous observations of TCCON FTS, GOSAT and LiDAR over Burgos. Aerosol scattering, when not properly considered, can be a significant source of error when retrieving X_{CO_2} from satellites [13–17]. Aerosols have also been shown to have an effect in the OCO-2 data, which will be briefly shown here under Section 3. We expect an improvement in the retrieval algorithm when actual profiles of cirrus clouds and stratospheric aerosols are taken into account.

For the purpose of GOSAT-2 product validation, we have developed a two-wavelength (532 and 1064 nm) polarization (532 nm) Mie and Raman (607 and 660 nm) LiDAR (hereafter we call "GOSAT-2 LiDAR") that is capable of observing vertical profiles of aerosols, thin cirrus clouds and water vapor (nighttime only) at the National Institute for Environmental Studies (NIES), Tsukuba, Japan. The GOSAT-2 LiDAR was installed in the TCCON container and was transported to the TCCON site in Burgos in December 2016. We assembled and adjusted the LiDAR system in January and February 2017. The detailed performance will be described in a separate manuscript dedicated to this LiDAR system, so only characteristics of the GOSAT-2 LiDAR are summarized in Table 1.

Table 1. Characteristics of GOSAT-2 LiDAR.

Transmitter				
Laser	Nd:YAG			
Wavelength	532 nm	1064 nm		
Pulse energy	210 mJ	180 mJ		
Pulse repetition rate	10 Hz			
Pulse width	5 ns	6 ns		
Beam divergence	0.1 mrad	0.1 mrad		
Receiver				
Telescope type	Advanced Coma-Free			
Telescope diameter	356 mm (f = 2845 mm)			
Field of view	1 mrad			
Center wavelength	532.05 nm	1064.18 nm	607.35 nm	660.45 nm
Polarization	P and S	None	None	None
Number of channels	3	1	1	1
Interference filter				
Bandwidth (FWHM)	0.32 nm	0.38 nm	0.25 nm	0.3 nm
Transmission	0.6	0.72	0.74	0.94
Detectors	PMT	APD	PMT	PMT
	(R3235-01)	(C30956EH)	(R3237-01MOD)	(R3237-01)
Quantum efficiency	0.08	0.68	0.06	0.04
Signal processing	16 bit A/D + Photon counting			
Time resolution	1 min			
Range resolution	7.5 m			
Maximum Range	120 km			

2.3. GOSAT and OCO-2 Data

For an initial comparison, we used X_{CO_2} satellite data from GOSAT and OCO-2. GOSAT X_{CO_2} was retrieved from the SWIR observations released as SWIR L2 product version 02.xx from NIES. Compared to the version 01.xx of the retrieval, this revised and improved version showed a much smaller bias and standard deviations of -1.48 and 2.09 ppm for X_{CO_2} with respect to the 13 TCCON stations studied in Yoshida et al. [16]. For the GOSAT soundings, we used strict coincidence criteria; within 400 km of the site and within 2 h of the TCCON measurements. This radius terminates just before the boundaries of metropolitan Manila and is away from the most densely populated areas. 50% of the radius is over ocean. With these criteria, we avoid measurements taken over strong CO_2 sources [11]. There are numerous measurements over the ocean using the satellite's glint mode that fulfill these criteria, however a small systematic bias in the glint data exists [18]. So for this study, we limit the data to retrievals over land. The glint mode retrievals will be investigated in later validation work.

NASA's Orbiting Carbon Observatory-2 (OCO-2) has been measuring X_{CO_2} in the Earth's atmosphere since July 2014 [19]. The observatory carries a three-channel imaging grating spectrometer and collects high-resolution spectra of reflected sunlight within the oxygen A-band near 0.76 µm, and within two carbon dioxide bands located near 1.6 µm and 2.0 µm, respectively [20]. The OCO-2 satellite is operated in three different viewing modes: nadir, glint, and target modes. Nadir and glint modes are considered as scientific modes whereas target mode is designed to evaluate the accuracy of the OCO-2 X_{CO_2} products by targeting validation sites. The OCO-2 bias correction procedure accounts for three different types of biases: footprint-dependent bias; spurious correlations of the retrieved X_{CO_2} with other retrieval parameters (parameter-dependent bias); and a scaling bias which ties OCO-2 X_{CO_2} to the WMO trace-gas standard scale [21] using TCCON data. TCCON data being tied to the WMO scale, serve as the link between the calibrated surface in situ measurements and the OCO-2 measurements (e.g., [22–24]). For more details on the OCO-2 bias correction see [25].

During a target-mode maneuver, the OCO-2 satellite rotates to point at a selected ground location. The spacecraft then scans across the site as it passes overhead to sweep across the ground several times.

After a period of about 5 min, the spacecraft transitions out of target mode back into its nominal science mode. The strength of target mode measurements is that thousands of spectra are obtained over a small region within a short time period. The targets are mostly selected where ground validation stations are located, typically at TCCON sites.

The Burgos TCCON station was selected as one of the sites for OCO-2 target mode observations and was specifically targeted on 21 April 2017. We use the OCO-2 version B7 retrospective data, available from GES-DISC (2016, http://disc.sci.gsfc.nasa.gov/OCO-2), and manually apply the filters listed in Wunch et al. [26] and footprint and parameter bias correction as described in Mandrake et al. [25]. Note, no scaling bias correction is applied to OCO-2 X_{CO_2} data at this point. We consider Burgos TCCON data to be coincident with the OCO-2 target-mode measurements when ground-based measurements have been recorded within $\pm$30 min of the time when the spacecraft is in target mode. Out of the 2788 target soundings we filtered, 841 were selected.

2.4. GEOS-Chem Tagged Tracer Simulations

To interpret the *CO* observations, the global 3-D chemical transport model GEOS-Chem v11-01 was used, driven by assimilated meteorological data from the Goddard Earth Observing System (GEOS) of the NASA Global Modeling and Assimilation Office (GMAO) MERRA-2 reanalysis. The offline *CO* sim ulation is described by Fisher et al. [27] and was run at $2^\circ \times 2.5^\circ$ horizontal resolution with 47 vertical levels, from January 2016 until the end of May 2017. Fossil fuel emissions globally were taken from EDGAR (Emission Database for Global Atmospheric Research) version 4.2 [28], with regional overwrites for Asia [29], Europe [30], Canada [31], the United States [32], and Mexico [33], along with biofuel emissions from Yevich and Logan [34], ship emissions from the International Comprehensive Ocean–Atmosphere Data Set (ICOADS) [35] and Aviation Emissions Inventory Code (AEIC) [36]. The simulations use the most recent emissions data available from each inventory; of most relevance here are the base emissions from EDGAR, which end in 2008, and the Asian emissions from MIX [29], which end in 2010. Biomass burning emissions are year-specific and come from the Quick Fire Emission Dataset-2 (QFED-2) [37]. Chemical production from methane and non-methane volatile organic compounds (NMVOC) is calculated using archived production rates from the full chemistry version of GEOS-Chem, with biogenic NMVOC emissions from the Model of Emissions of Gases and Aerosols from Nature (MEGAN) version 2.1 [38]. We use regional tracers from the *CO* simulation to identify sources of observed enhancements recorded in the TCCON data. Because we are interested in the sources of variability rather than absolute concentrations, we first correct a known low bias in the GEOS-Chem *CO* simulation, driven at least in part by a high bias in global OH [27]. We calculate an offset using a weighted least squares fit of the GEOS-chem output to the TCCON data, computed only on days when both model and observations suggest the site is sampling clean background air from the Pacific. The resultant offset of 4.9 ppb is then applied to all GEOS-Chem output.

2.5. Backward Trajectories

To identify the origin of the aerosols and the *CO*, three-dimensional backward trajectories of air parcels were calculated with the trajectory ensemble option of the NOAA Hybrid Single Particle Lagrangian Integrated Trajectory (HYSPLIT) model [39]. The trajectory ensemble option provides a multiple trajectory approach wherein the model starts multiple trajectories from the same starting location. Each member of the trajectory ensemble is then calculated by offsetting the meteorological data by a fixed grid factor (one meteorological grid point in the horizontal and 0.01 sigma units in the vertical). This results in 27 members for all-possible offsets in X, Y, and Z. The divergence of those trajectories would provide a more quantitative estimate of the uncertainty associated with the center point trajectory (source: http://ready.arl.noaa.gov/hypub-bin/trajtype.pl?runtype=archive, HYSPLITtutorial).

3. Results

3.1. Time Series of X_{CO_2}, X_{CH_4}, X_{H_2O} and X_{CO}

Measurements following TCCON protocols commenced on 3 March 2017. The retrieved X_{CO_2}, X_{CH_4}, X_{H_2O} and X_{CO} using the GGG2014 software are shown in Figure 1. The shown time series extends from that day to 30 June 2017, and have continued since then. A spike in X_{CH_4}, which is the highest value in this record, can be seen in early March (8–9 March). A spike on the same days can also be seen in the X_{CO_2} but is less prominent. This episode is also evident in the X_{CO} and also the highest measured in the time series. *CO* is primarily produced from biomass burning, oxidation of CH_4 and other biogenic hydrocarbons, and fossil fuel combustion. It has a lifetime ranging from weeks to a few months, which makes it an effective indicator of how transport processes distribute atmospheric pollutants from biomass burning and fossil fuel combustion on a global scale [40]. Towards the end of June, we sampled low values of X_{CO} (<70 ppb), close to "clean surface air" mole fractions of 60 ppb measured by Ridder et al. [41] using ship-based in situ FTIR in the Western Pacific. We further investigate this tracer in the GEOS-Chem results below. The measurements shown in Figure 1 covered the dry season and the beginning of the rainy season (southwest monsoon). The onset of the monsoon could be discerned from the increase in the water vapor (X_{H_2O}) starting around mid-May.

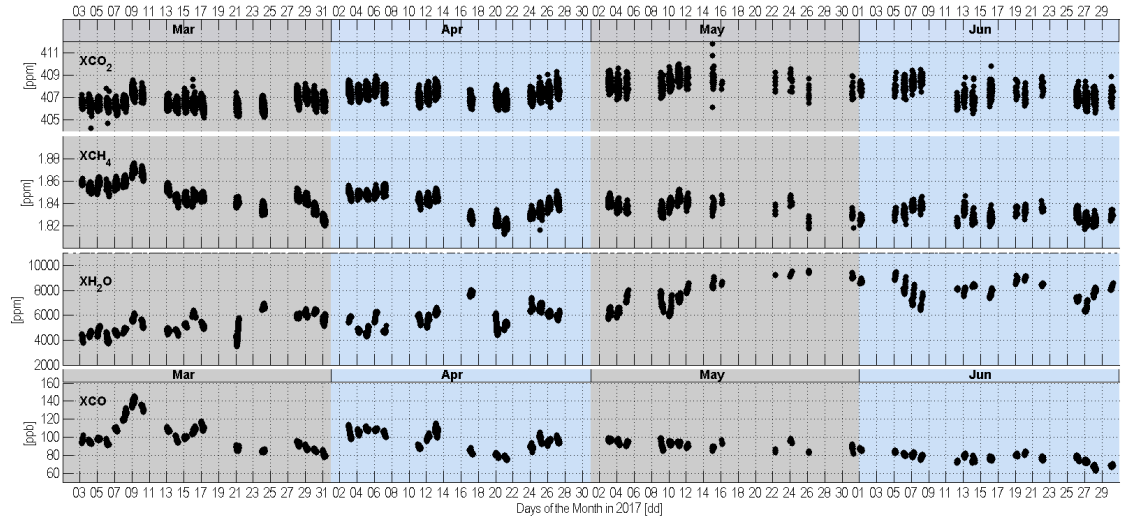

Figure 1. Retrieved column-averaged dry air mole fractions of CO_2, CH_4 , H_2O and X_{CO} from the TCCON station in Burgos, Ilocos Norte, Philippines.

3.2. OCO-2, GOSAT and TCCON Comparisons

All current space-based X_{CO_2} measurements have systematic biases [26]. Recently, Wunch et al. [26] made a comparison between the first major release of the OCO-2 retrieval algorithm (B7r) and X_{CO_2} from TCCON, OCO-2's primary ground-based validation network. Wunch et al. [26] reported absolute median differences of less than 0.4 ppm and RMS differences of less than 1.5 ppm. Wunch et al. [26] calculated a best fit line from the X_{CO_2} measured by OCO-2 vs. TCCON to show consistency over all target mode observations at the TCCON sites. Here, we extend the comparisons done by Wunch et al. [26] by adding the measurements in Burgos.

Figure 2 shows OCO-2 X_{CO_2} target-mode data comparisons with coincident TCCON data for the TCCON sites in Tsukuba (Japan), Wollongong and Darwin (both Australia), and Burgos (Philippines). The best fit line (solid line) was computed as described [26] for the time period spanning 8 September 2014 through 24 July 2017, including a total of 164 target mode observations at 21 different TCCON

sites (not shown here for clarity). The scaling factor of 0.99755 ± 0.00107 is slightly different to the factor derived in Wunch et al. [26] (0.9977) due to the increasing number of target mode observations with time. Our initial analysis shows that the comparison between Burgos TCCON measurements and coincident OCO-2 target mode observations is in good agreement with the best fit line. Ideally, the X_{CO_2} retrieved by OCO-2 vs. The X_{CO_2} measured at the Burgos TCCON station during the target maneuver would lie on the 1:1 line (dashed grey line), but the fact that they lie in the same best fit line calculated by [26] supports the overall consistency of the TCCON network. The mean bias between OCO-2 and Burgos TCCON X_{CO_2}, during this OCO-2 target mode overpass, is 0.83 ± 1.22 ppm (TCCON: 406.76 ± 0.36 ppm; OCO-2: 405.93 ± 1.17 ppm). It is obvious in Figure 2 that there are two outliers from the TCCON station in Wollongong, Australia. The reason for this is probably due to the presence of stratospheric aerosols caused by the eruption of the Calbuco volcano on 22 April 2015 [42].

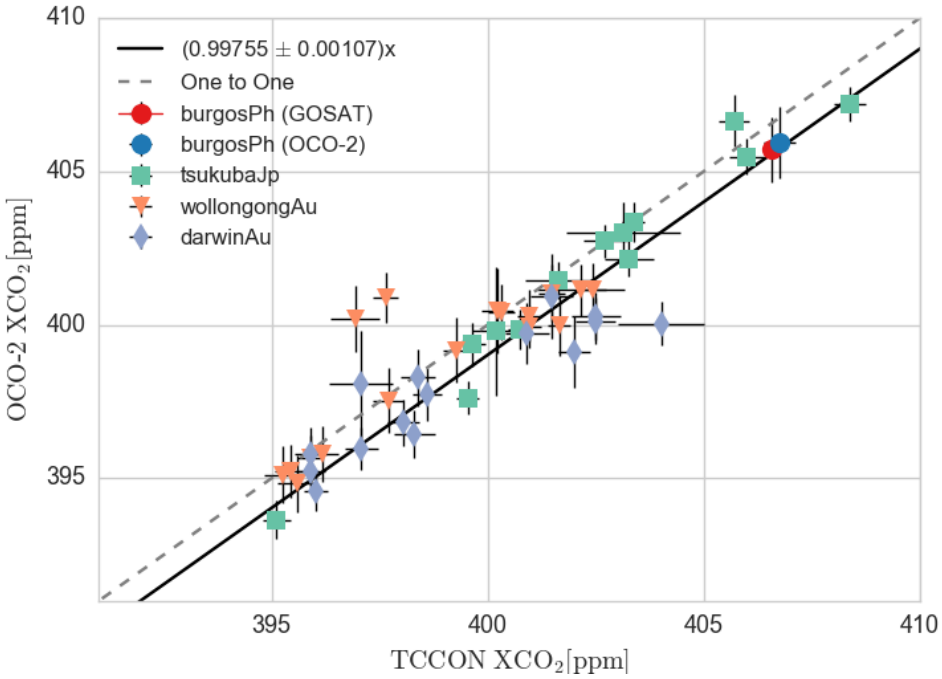

Figure 2. Target mode X_{CO_2} retrievals from the OCO-2 satellite vs. X_{CO_2} from TCCON stations. Only stations in Tsukuba, Wollongong, Darwin and Burgos are shown for clarity. The calibration line (solid black line) is derived from all TCCON sites. The most recent GOSAT sounding (red circle) is also added on this plot, but not included in the calculation of the calibration curve. It falls within 0.13 ppm of the OCO-2 calibration line. The two outliers in the OCO-2 measurements over Wollongong (downward triangles) are probably due to bias induced by stratospheric aerosols caused by the eruption of the Calbuco volcano on 22 April 2015 [42].

Irregular surface properties (e.g., brightness, slope) have been known to induce bias in the X_{CO_2} retrievals from space (e.g., [3,26]). Due to the irregular topography of Luzon Island (mountains, forests, rice fields and adjacent ocean), targeted observations from GOSAT are spatially limited and would oftentimes be contaminated by clouds, especially close to the rainy season. GOSAT does not perform the same targeting method as OCO-2. That is why there are few GOSAT retrievals available over land within this time period. On 8 March 2017 at 13:08 local time (05:08 UTC), we were able to get a nearest sounding from GOSAT at 324.34 km from the TCCON site (great circle distance), which fulfilled our satellite coincidence criteria. The GOSAT X_{CO_2} retrieval yielded a value of 405.71 ± 1.04 ppm. The TCCON-GOSAT measurement difference was 0.86 ± 1.06 ppm. Using the calibration line from

the OCO-2 observations (i.e., satellite X_{CO_2} = 0.99755 × TCCON), we arrive at a value of 405.57 ppm during the GOSAT overpass, which is a difference of 0.13 ppm from the actual GOSAT X_{CO_2} retrieval.

3.3. LiDAR Results

We started LiDAR observations in January 2017. Figure 3 shows time-altitude cross sections of backscattering ratio R and total volume depolarization ratio D at 532 nm over Burgos for 1–16 March 2017. In this case, the LiDAR signals were averaged for 3 h with 60 m altitude range resolution. Aerosols and cumulus clouds were observed below 4 km, and optically thick aerosols were observed from 7 March to 10 March. Based on the values of D, cirrus clouds were occasionally present in the altitude range of 11–17 km.

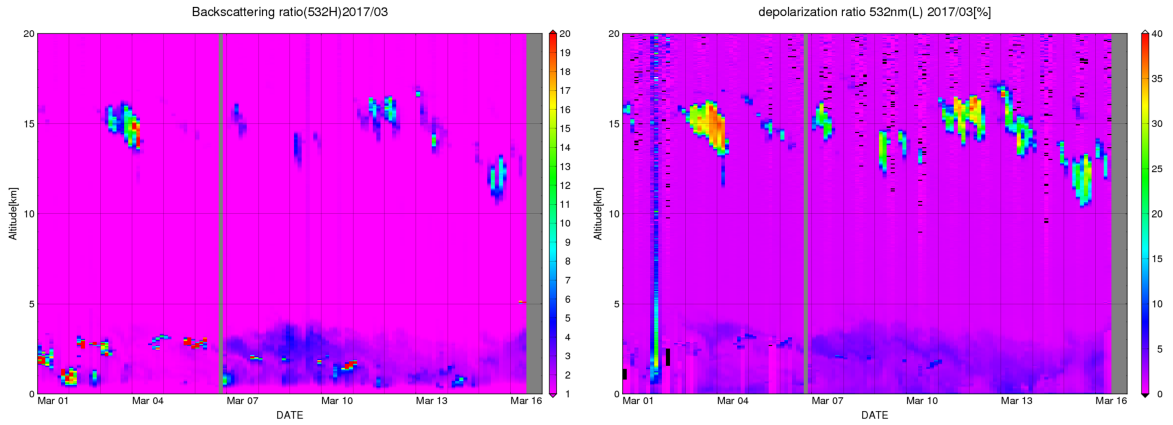

Figure 3. Time-Altitude transects of LiDAR backscatter and depolarization signals, dates are in local time (LT).

The vertical profiles of R at 532 nm for 5–35 km observed over Burgos on 26 January and 28 February 2017 are shown in Figure 4. To calculate R, we used the Japanese 55-year Reanalysis (JRA-55) data [43]. The maximum values of R (R_{max}) of stratospheric aerosols were 1.14 at 25.0 km on 26 January and 1.16 at 29.2 km on 28 February.

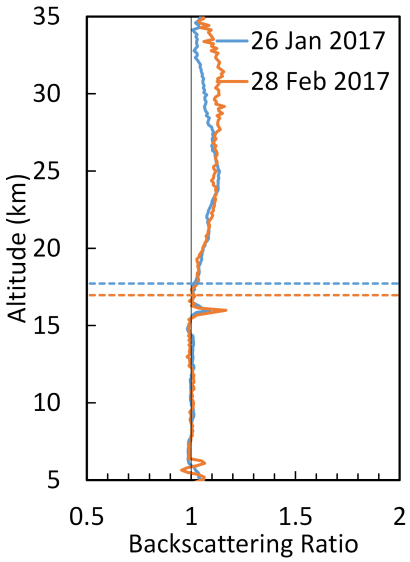

Figure 4. Backscattering ratio (R) profiles at 532 nm observed over Burgos on 26 January 2017 and 28 February 2017. The dashed lines represent the tropopause levels at 17.7 km and 17.0 km for the respective days.

To calculate the stratospheric AOD, we integrated the backscattering coefficients starting from the tropopause levels (dashed lines) up to 33 km. The integrated backscattering coefficients (IBCs) of stratospheric aerosols from the tropopause level to 33 km were 6.81×10^{-5} sr and 7.58×10^{-5} sr on 26 January and 28 February, respectively. From here, we determined the stratospheric AOD by assuming that the LiDAR ratio for stratospheric aerosols is 50 sr^{-1} [44]. This yields stratospheric AODs of 0.0034 on 26 January and 0.0038 on 28 February 2017.

Figure 5 shows vertical profiles of several quantities measured by the LiDAR with a resolution of 150 m over Burgos on 8 March 2017 at 21:00–23:59 local time (LT). These quantities are: R at 1064 nm and 532 nm, backscatter-related Ångström exponent (BAE), particle depolarization ratio (DEPp), extinction-to-backscatter ratio (i.e., LiDAR ratio or LR) and water vapor mixing ratio. The definitions of these LiDAR physical quantities are denoted in [36]. The lowest altitude of the LiDAR measurement was 700 m due to imperfect overlap of the transmitter-receiver optical alignment of the LiDAR system.

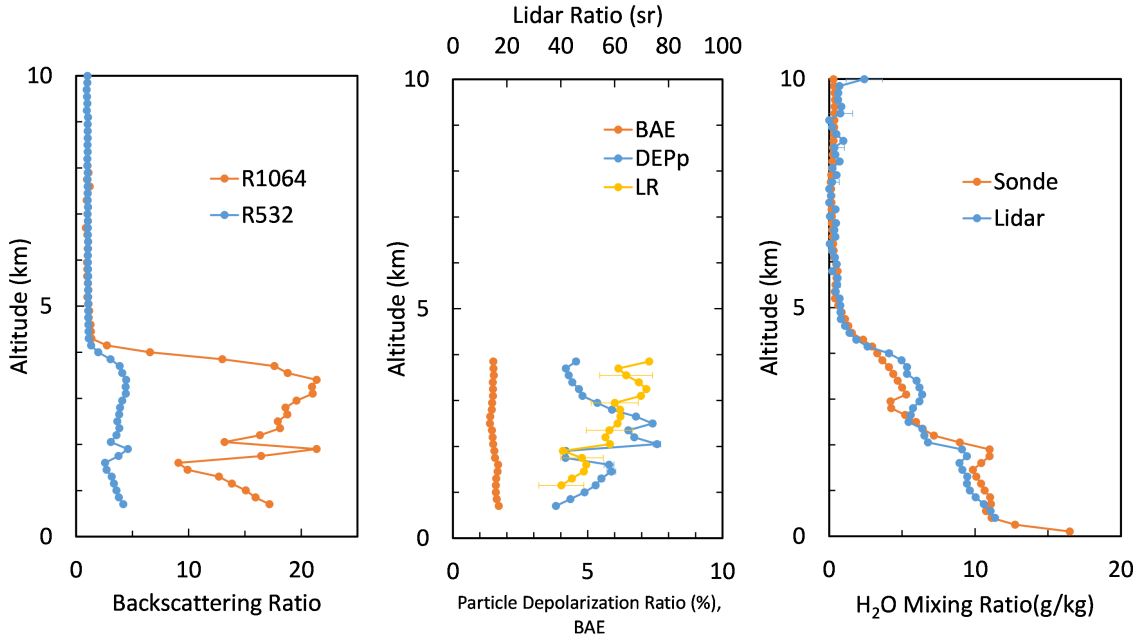

Figure 5. Vertical profiles of backscattering ratios at 1064 nm (R1064) and 532 nm (R532) (**left**), backscatter-related Ångström exponent (BAE), particle depolarization ratio (DEPp), LiDAR ratio (LR) (**center**) and water vapor mixing ratio measured by LiDAR and radiosonde (but over Laoag) (**right**) over Burgos on 8 March 2017. Horizontal bars represent the error bars of respective physical quantities.

Based on R, an aerosol layer extended up to about 4.5 km. We find peak values of R existing at 3.4 km (4.4 at 532 nm and 22 at 1064 nm). The aerosol optical depth (AOD) at 532 nm was 0.75 ± 0.13 in the altitude range of 0.035–10 km (R at 0.7 km was extrapolated down to the ground level). We detected non-spherical particles that probably co-existed with spherical particles because the DEPp values were 4–8%. At 1.1–3.8 km, the mean value of LR at 532 nm was 58 ± 10 sr and the BAE was 1.4–1.7.

For the water vapor Raman LiDAR, we used the calibration constant determined on 26 January (Figure 4). Figure 5 (rightmost panel) shows the comparison of the radiosonde-derived water vapor mixing ratio with the LiDAR data on 8 March at 22:00 LT over Laoag. It is shown here that the vertical distribution of water vapor mixing ratio measured by LiDAR was consistent with that observed by radiosonde. The measurements also show a very low mixing ratio of water vapor at 6–9 km altitude, suggesting a dry free troposphere above the aerosol layer.

LiDAR observations stopped from 17 March 2017 because the high solar elevation at noon would cause sunlight to be directly received by the telescope, cause optical misalignment of the LiDAR system

and damage optical components. LiDAR observations start again in late September 2017. Based on the simultaneous observations of TCCON FTS, GOSAT and LiDAR over Burgos, we plan to further investigate the influence of the tropospheric aerosols and cirrus clouds on the most recent GOSAT data (ver.02.72) which will be released soon.

3.4. HYSPLIT Backward Trajectories

Backward trajectories calculated from HYSPLIT on 8 March 2017 using the ensemble option are displayed in Figure 6. The starting time coincides with the LiDAR profiles on Figure 4 and with the time when the *CO* is just starting to rise to reach the maximum on 9 March. The backward trajectories were started at altitudes of 700 m (Figure 6a) and 2000 m (Figure 6b) over the Burgos site and ran backwards for 5 days from 15:00 UTC (23:00 LT) on 8 March 2017. The trajectories indicate that aerosols at about 700 m observed over Burgos were mainly transported from East Asia and those at about 2000 m from East Asia and South Asia.

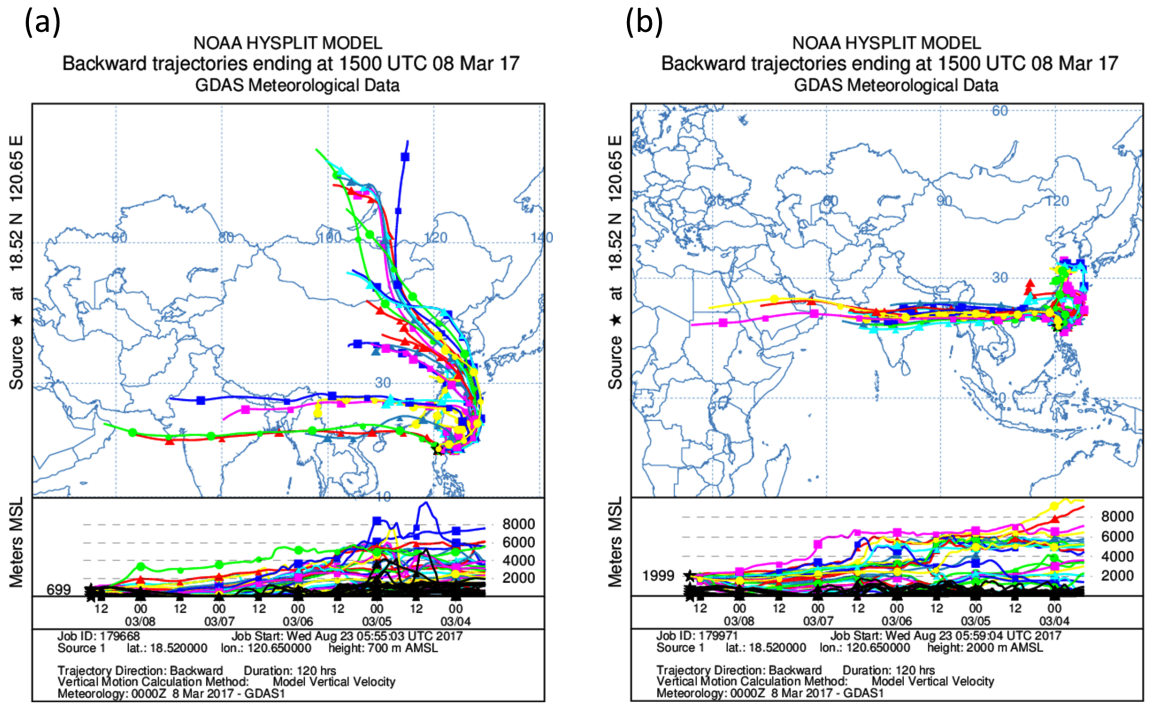

Figure 6. The 120-h HYSPLIT model backward trajectory of 27 air parcels (colors) and terrain height (black line) from Burgos at (**a**) 700 m and (**b**) 2000 m above sea level (a.s.l) ending at 15:00 UTC on 8 March 2017.

3.5. GEOS Chem CO Comparisons with TCCON Data

As discussed in Section 2.4, we corrected a known low bias in the GEOS-Chem *CO*, because we are interested in the sources of variability rather than absolute concentrations. The resultant offset of 4.9 ppb is applied to all GEOS-Chem output. This is shown in Figure 7. The TCCON measurements of X_{CO} are shown as blue dots and the corresponding model simulations with the offset applied are shown as red squares. The larger scale temporal variability of X_{CO} (weeks) is well captured by GEOS-Chem in this figure, but a low bias still exists, especially when the X_{CO} is enhanced with respect to the clean background. Moreover, the variability in the observations is larger than that of the model even after offset correction. A possible reason for this is the model's spatial resolution, which tends to smooth out the signals from scattered point sources. Local, sporadic *CO* sources such as waste and agricultural burning in the region may also contribute. Figure 8 shows surface *CO* from the

GEOS Chem model simulated on 8 March 2017 at 05:00 UTC. The red "blob", representing surface *CO* concentrations over 400 ppb, hovers around Hanoi, the Pearl River delta and the provinces West, Northwest of it. The Philippines is in the middle of the interface where the clean Western Pacific air (dark shade to black) meets the East Asian outflow of pollution. Wind speeds and directions are shown as streamlines.

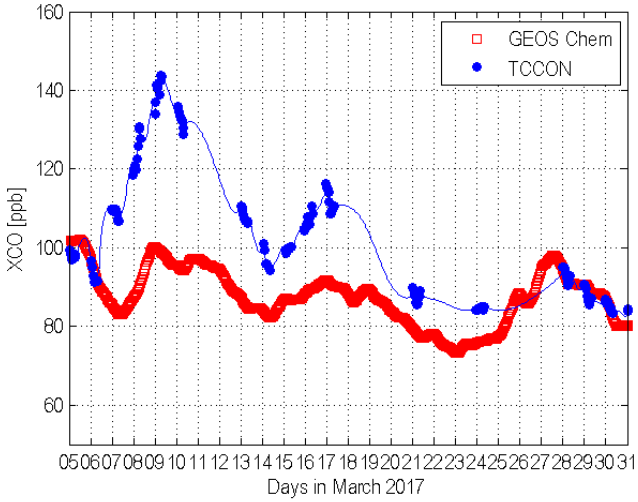

Figure 7. TCCON measurements of X_{CO} (**blue**) and the corresponding model simulations (**red**, offset applied).

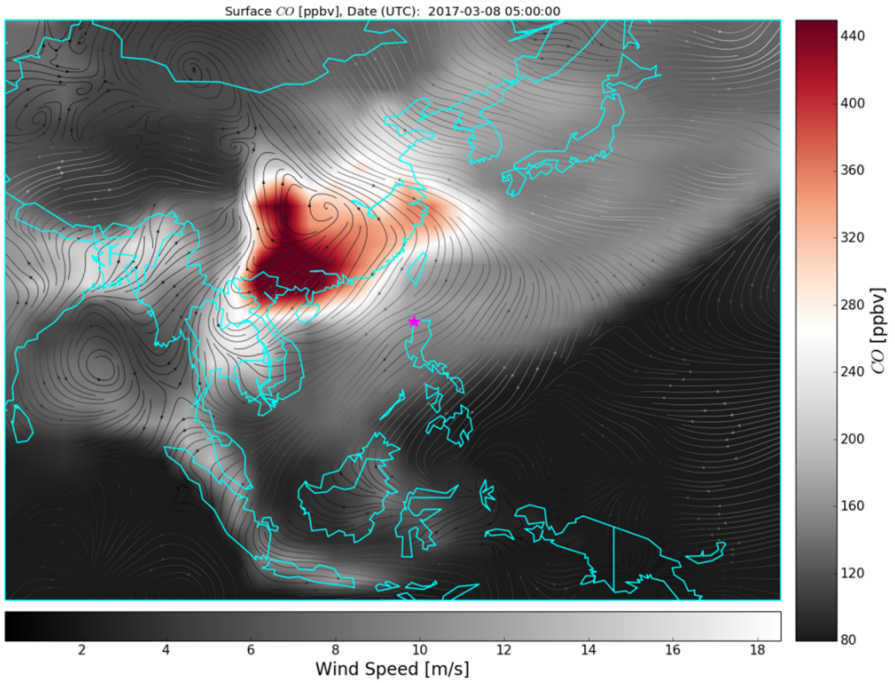

Figure 8. Surface *CO* (color shaded from black to red) from the GEOS Chem model simulated on 8 March 2017 at 05:00 UTC. The Philippines is right in the middle of the interface where the clean Western Pacific air (dark shade to black) meets the East Asian outflow of elevated *CO*. Wind speeds and direction are shown as streamlines. The location of the TCCON station in Burgos is marked by the magenta star.

3.6. Tagged Tracer Simulations

A graph of the contributions to the *CO* using the tagged tracer simulations is shown in Figure 9. Shown here are contributions from fossil fuels and biomass burning from the northern and southern hemisphere, biomass burning from Indonesia, and oxidation from CH_4 and non-methane volatile organic compounds (NMVOC). CH_4 oxidation provides a steady background of roughly 30 ppb but northern hemisphere fossil fuel emissions (black line) account for the large enhancements in the *CO*. Figure 10 shows a snapshot of the fossil fuel contribution to the surface *CO* concentrations used in the tagged tracer simulations for March 2017. We see high concentrations in East Asia, where winter haze conditions in large city clusters (e.g., Guangzhou) could have average PM2.5 concentrations that are approximately one to two orders of magnitude higher than those observed in urban areas in the US and European countries [45].

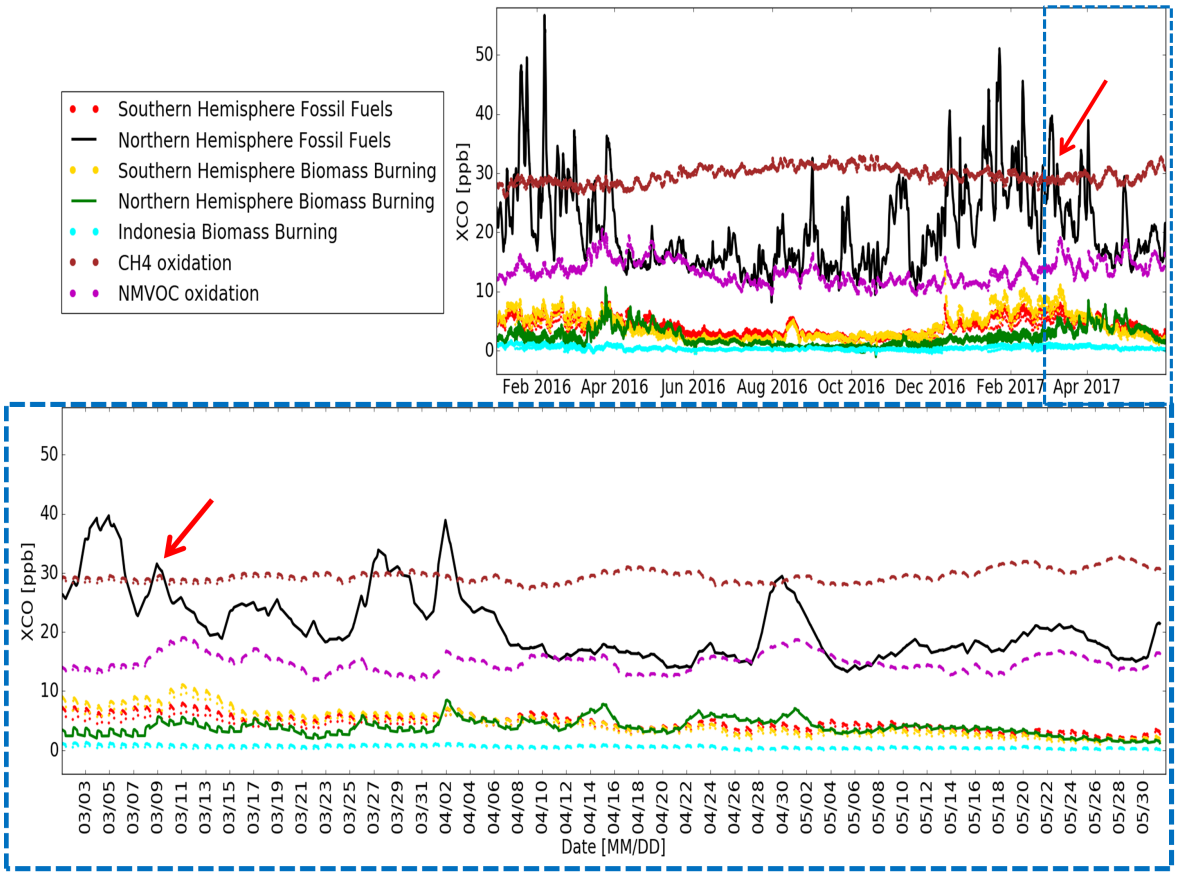

Figure 9. Top right: Tagged tracer simulations of *CO* from GEOS Chem for January 2016 to May 2017. This plot shows the contribution of different sources to the column averaged dry air mole fractions of *CO* at the TCCON site in Burgos. The bottom plot shows a zoom-in on March–May 2017. The inundation in the X_{CO} is dominated by the fossil fuel signals ("Northern Hemisphere Fossil Fuels", black line), which are mostly from East Asia (Figure 8), especially on 9 March (indicated by the red arrow). The background contributions from CH_4 and NMVOC oxidation are significant but the enhancements are much less. The biomass burning signals from South America, Africa and Indonesia around March contribute little in this region.

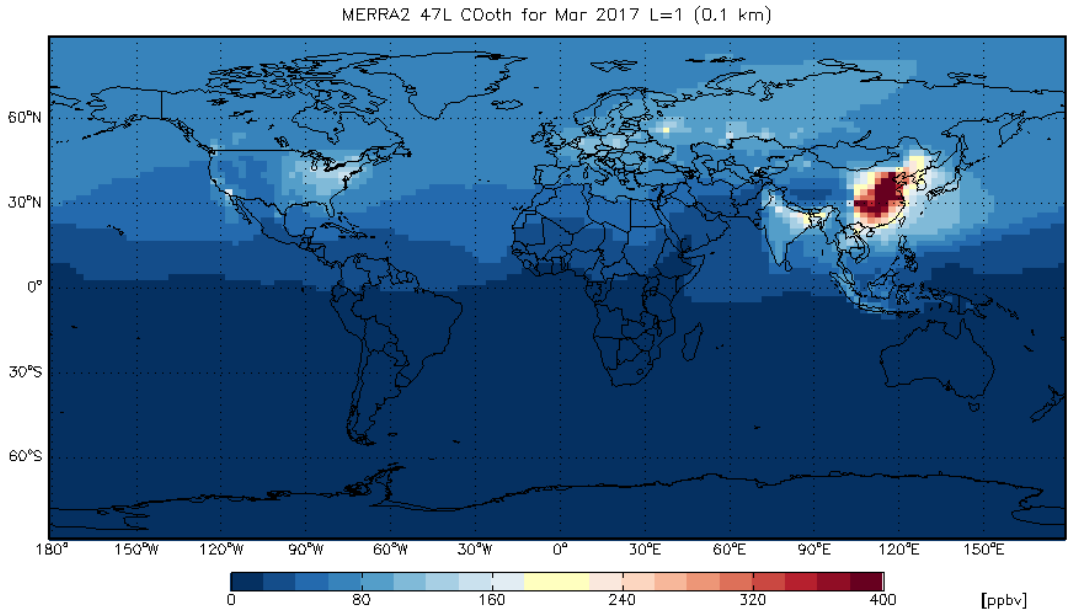

Figure 10. A snapshot of the fossil fuel contribution to the surface *CO* concentrations used in the tagged tracer simulations for March 2017.

4. Discussion

The TCCON dataset presented here contains retrievals of X_{CO_2}, X_{CH_4}, X_{H_2O} and X_{CO} since 3 March 2017. These are the first measurements from the ground of column-averaged DMFs of these gases in Southeast Asia, following TCCON standards. Most evident in the column-averaged DMFs is the X_{CO} "surge", which had a peak on 8–9 March. This was the highest X_{CO} value in the time series that extends until 30 June in this study. Small peaks coinciding with the *CO* peak can also be noticed in the X_{CH_4} and X_{CO_2} and less prominently in the X_{H_2O}.

The southwest monsoon (SWM) season (rainy season) started during the last week of May in the Philippines. This is per definition, marked by 5 consecutive days of rainfall measured by weather stations in Western Luzon, according to the local Weather Bureau (PAGASA). The onset of the rainy season is manifested in the measured XH_2O, which markedly increased around mid-May and continues to be higher relative to the March–April values until the end of the current time series. This also signals the migration of the inter-tropical convergence zone (ITCZ), which was south of the site in January and moves north of the site by July. The flow reversal to northeast monsoon (typically dryer, cooler months) usually does not take place until mid-October [46].

The GOSAT sounding used here was taken at the coordinates 15.6123°N, 120.8916°E, which are mostly rice fields that are flat, homogeneous and dry at this time of the year. We also do not expect any significant CO_2 sequestration or emissions from the dry rice fields, as demonstrated by Lasco et al. [47]. The nearest large city to this satellite footprint is Cabanatuan City (pop. 302,000), 24 km away by road. This location is far away and located upwind from large CO_2 sources (e.g., the city of Manila, coal-fired power plants, etc.). Unfortunately, we were not able to obtain more GOSAT soundings but this will improve in the future with the availability of more data, especially from GOSAT-2. In GOSAT-2, the "active re-point targeting system" (intelligent pointing system) will be installed in order to increase the opportunity for clear sky observation frequency [48]. Nevertheless, the comparison with the satellite data looks very promising. The GOSAT measurement falls within 0.13 ppm of the calibration line derived from the OCO-2 vs. TCCON targets.

Tagged tracer simulations can be used to examine the drivers of the variability in the measured X_G at the TCCON site e.g., [49]. Based on the GEOS-Chem tagged tracer simulations that we employed

here, the *CO* peak seen in 8–9 March over Burgos is likely to result mostly from fossil fuel emissions, which are dominated by emissions from East Asia, having little influence from biomass burning. Biomass burning from Asia started to contribute to a noticeable signal in mid to late April. This confirms the study of Liu et al. [50] during the TRACE-P aircraft mission in February–April 2001, where it was shown that in spring, "boundary layer outflow over the western Pacific is largely devoid of biomass burning influence". Interestingly, Figure 7 of Liu et al. [50] is very similar to Figure 8 here (i.e., Liu et al. [50] showed surface *CO* for 9 March 2001). The patterns are very similar, except in the magnitude of East Asian surface *CO*, probably due to increase in industrial activity in the past 16 years.

We can see from Figure 3 (right panel), that there is a persistent particle depolarization signal of about 4–5% at 532 nm below 5 km during the first half of March. Particle depolarization is an indicator for non-sphericity of particles [51], i.e., large values indicate the presence of non-spherical particles, such as dust or ice crystals. For instance, the presence of Asian dust could yield values of 20% [52]; however, this optical property can be influenced by the presence of water vapor, modulated by temperature e.g., [53], i.e., the signals can be dampened or heightened by the presence of water vapor. Heese et al. [54] reported linear particle depolarization ratios with values below 5%, with a mean value of $3.6 \pm 3.7\%$ for urban pollution particles mixed with particles produced from biomass and industrial burning above the Pearl River Delta. The depolarization signals we measured may have been closer to those reported by Heese et al. [54], i.e., a mix of particles from biomass and industrial burning. Also, following an analysis from Uchino et al. [44], the main aerosol component we detected in this period might have been sub-micrometer-sized spherical particles, because the depolarization signal was small and the backscatter-related Ångström exponent is on the order of 1–2 (Figure 5, middle panel).

5. Conclusions

Here, we presented the first TCCON retrievals of trace gases and water vapor Raman LiDAR measurements at the TCCON station in Burgos, Ilocos Norte, Philippines. The TCCON retrievals comprise of column-averaged dry air mole fractions of CO_2, CH_4, H_2O and CO. The LiDAR measurements included backscattering ratios at 1064 nm and 532 nm, backscatter-related Ångström exponent (BAE), particle depolarization ratio (DEPp), LiDAR ratio (LR), water vapor mixing ratio and calculations of aerosol optical depth (AOD).

Satellite measurements of X_{CO_2} from GOSAT and OCO-2 show excellent agreement with this TCCON site. To ascertain the differences, more coincidences and target observations spanning different seasons are necessary. This will improve in the future as we continue to operate and as GOSAT-2 measures in orbit in 2018/2019. Our initial analysis here also shows that the comparisons between GOSAT, coincident OCO-2 target mode observations, and Burgos TCCON are in good agreement with the best fit line derived from 164 OCO-2 target mode observations at 21 different TCCON sites.

Possible pollution plumes were detected and our data in this study point to its origins from fossil fuel combustion in continental East Asia. This confirms analysis of the surface influence functions in Belikov et al. [55] and Velazco et al. [11], showing that the location of this TCCON site measures air with significant and variable contributions from emissions of some of the largest anthropogenic carbon sources in the world. The location also allows for sampling of relatively clean background air from the western Pacific that could serve as baseline measurements to isolate signals of strong GHG sources.

Acknowledgments: The TCCON Philippines project is supported in part by the GOSAT-2 project of Japan. Retrieval processing for GOSAT SWIR L2 was conducted at the Research Computation Facility for GOSAT-2. We also thank the Japanese Ministry of Environment. We acknowledge the tremendous support from EDC, especially from F. R. Lopez, O. M. Lopez, R. B. Tantoco, A. de Jesus, EDC board members, J. Russell, OML Center for Climate Change and First Philippine Holdings. Special thanks to Art Valdez. Site support is also generously provided by R. Chua, A. Durog, C. Aguilar and all EBWPC staff. We also thank the government of Ilocos Norte. The authors also thank NIES for providing GOSAT data via the GOSAT RA projects (V. Velazco [RA8]). We thank NASA for providing the OCO-2 retrospective data, available from GES-DISC. We thank F. Schwandner, G. Ostermann, A. Eldering, D. Crisp and the rest of the OCO-2 team for facilitating the target mode observations. We thank PAGASA-DOST for the Met-Hydro Decision Support Infosys website for daily weather information.

We acknowledge support from TCCON partners especially Debra Wunch, Geoffrey C. Toon, Paul O. Wennberg. Funding is provided in part by the Australian Research Council (ARC) for TCCON (DP160101598, DP140101552, DP110103118) and University of Wollongong SMAH-UIC International Links Grant Scheme for travel support granted to Velazco. This research was undertaken with the assistance of resources from the NCI National Facility systems at the Australian National University through the National Computational Merit Allocation Scheme supported by the Australian Government. B. Bukosa would like to acknowledge support from both the ARC and the University of Wollongong. N. Deutscher acknowledges support from ARC-DECRA (DE140100178). We thank Jenny A. Fisher for valuable discussions and help with GEOS-Chem and the tagged tracer studies. We thank the three anonymous referees for providing valuable reviews that helped improve this manuscript.

Author Contributions: V.A.V. conceived the manuscript, processed and analyzed TCCON data, calculated the satellite coincidences (GOSAT), determined the GEOS-Chem offset and was involved in instrument set-up and Burgos operations. I.M. is the TCCON instrument PI and led the set-up of the NIES FTS container system, is involved in day-to-day operations and pre-processing of level 0 data and data analysis. A.H. is the dedicated instrument engineer responsible for instrument set-up, day-to-day operations and pre-processing of level 0 data. O.U. is the LiDAR PI and leads the LiDAR set-up, operations and wrote the LiDAR results and analysis sections. T.S., T.I., T.N. are all involved in LiDAR instrument set-up and data analysis. G.B. contributed to the LiDAR operations and provided weather data. Y.Y. processed and provided advanced Level 2 GOSAT data. M.K. did the OCO-2 data processing, bias correction and TCCON comparisons, wrote the OCO-2 section. B.B. did the modeling (CO and CH_4, CO_2), contributed to the analysis and wrote the GEOS-Chem chapter. N.D. contributed to the GEOS Chem tagged tracers analysis and provided valuable inputs. D.G. guided the TCCON instrument set-up, helped with measurements, set the preprocessing routines up and contributed to the data analysis. All authors read and provided comments on the manuscript.

Conflicts of Interest: The authors declare no conflict of interest. The founding sponsors had no role in the design of the study; in the collection, analyses, or interpretation of data; in the writing of the manuscript, and in the decision to publish the results.

References

1. AccessScience. Available online: https://doi.org/10.1036/1097-8542.BR0612171 (accessed on 4 September 2017).
2. Wunch, D.; Toon, G.C.; Blavier, J.F.L.; Washenfelder, R.A.; Notholt, J.; Connor, B.J.; Griffith, D.W.T.; Sherlock, V.; Wennberg, P.O. The Total Carbon Column Observing Network. *Philos. Trans. R. Soc. A Math. Phys. Eng. Sci.* **2011**, *369*, 2087–2112.
3. Kuze, A.; Suto, H.; Nakajima, M.; Hamazaki, T. Thermal and near infrared sensor for carbon observation Fourier-transform spectrometer on the Greenhouse Gases Observing Satellite for greenhouse gases monitoring. *Appl. Opt.* **2009**, *48*, 6716.
4. Nakajima, M.; Kuze, A.; Suto, H. The current status of GOSAT and the concept of GOSAT-2. In *Sensors Systems, and Next-Generation Satellites XVI*; Meynart, R., Neeck, S.P., Shimoda, H., Eds.; SPIE: Bellingham, WA, USA, 2012.
5. Boesch, H.; Baker, D.; Connor, B.; Crisp, D.; Miller, C. Global characterization of CO_2 column retrievals from Shortwave-Infrared Satellite Observations of the Orbiting Carbon Observatory-2 Mission. *Remote Sens.* **2011**, *3*, 270–304.
6. Eldering, A.; Kaki, S.; Crisp, D.; Gunson, M.R. The OCO-3 Mission. In Proceedings of the AGU Fall Meeting 2013, San Francisco, CA, USA, 9–13 December 2013.
7. Ingmann, P.; Yasjka Meijer, B.V. Status overview of the GMES Missions Sentinel-4, Sentinel-5 and Sentinel-5p. In Proceedings of the ATMOS 2012—Advances in Atmospheric Science and Applications, Bruges, Belgium, 18–22 June 2012.
8. Cressot, C.; Chevallier, F.; Bousquet, P.; Crevoisier, C.; Dlugokencky, E.J.; Fortems-Cheiney, A.; Frankenberg, C.; Parker, R.; Pison, I.; Scheepmaker, R.A.; et al. On the consistency between global and regional methane emissions inferred from SCIAMACHY, TANSO-FTS, IASI and surface measurements. *Atmos. Chem. Phys.* **2014**, *14*, 577–592.
9. Agency, I.E. Available online: http://www.iea.org/publications/freepublications/publication/WEO2015_SouthEastAsia.pdf (accessed on 4 September 2017).
10. Rayner, P.J.; Utembe, S.R.; Crowell, S. Constraining regional greenhouse gas emissions using geostationary concentration measurements: A theoretical study. *Atmos. Meas. Tech.* **2014**, *7*, 3285–3293.
11. Velazco, V.; Morino, I.; Uchino, O.; Deutscher, N.; Bukosa, B.; Belikov, D.; Oishi, Y.; Nakajima, T.; Macatangay, R.; Nakatsuru, T.; et al. Total carbon column observing network Philippines: Toward quantifying atmospheric carbon in southeast asia. *Clim. Disaster Dev. J.* **2017**, *2*, 1–12.

12. Wunch, D.; Toon, G.C.; Sherlock, V.; Deutscher, N.M.; Liu, C.; Feist, D.G.; Wennberg, P.O. *The Total Carbon Column Observing Network's GGG2014 Data Version*; Technical Report; Carbon Dioxide Information Analysis Center, Oak Ridge National Laboratory: Oak Ridge, TN, USA, 2015.
13. Guerlet, S.; Butz, A.; Schepers, D.; Basu, S.; Hasekamp, O.P.; Kuze, A.; Yokota, T.; Blavier, J.F.; Deutscher, N.M.; Griffith, D.W.; et al. Impact of aerosol and thin cirrus on retrieving and validating XCO2 from GOSAT shortwave infrared measurements. *J. Geophys. Res. Atmos.* **2013**, *118*, 4887–4905.
14. Morino, I.; Uchino, O.; Inoue, M.; Yoshida, Y.; Yokota, T.; Wennberg, P.O.; Toon, G.C.; Wunch, D.; Roehl, C.M.; Notholt, J.; et al. Preliminary validation of column-averaged volume mixing ratios of carbon dioxide and methane retrieved from GOSAT short-wavelength infrared spectra. *Atmos. Meas. Tech.* **2011**, *4*, 1061–1076.
15. Uchino, O.; Kikuchi, N.; Sakai, T.; Morino, I.; Yoshida, Y.; Nagai, T.; Shimizu, A.; Shibata, T.; Yamazaki, A.; Uchiyama, A.; et al. Influence of aerosols and thin cirrus clouds on the GOSAT-observed CO_2: A case study over Tsukuba. *Atmos. Chem. Phys.* **2012**, *12*, 3393–3404.
16. Yoshida, Y.; Kikuchi, N.; Morino, I.; Uchino, O.; Oshchepkov, S.; Bril, A.; Saeki, T.; Schutgens, N.; Toon, G.C.; Wunch, D.; et al. Improvement of the retrieval algorithm for GOSAT SWIR X_{CO_2} and X_{CH_4} and their validation using TCCON data. *Atmos. Meas. Tech.* **2013**, *6*, 1533–1547.
17. Ohyama, H.; Kawakami, S.; Tanaka, T.; Morino, I.; Uchino, O.; Inoue, M.; Sakai, T.; Nagai, T.; Yamazaki, A.; Uchiyama, A.; et al. Observations of X_{CO_2} and X_{CH_4} with ground-based high-resolution FTS at Saga Japan, and comparisons with GOSAT products. *Atmos. Meas. Tech.* **2015**, *8*, 5263–5276.
18. Zhou, M.; Dils, B.; Wang, P.; Detmers, R.; Yoshida, Y.; O'Dell, C.W.; Feist, D.G.; Velazco, V.A.; Schneider, M.; De Mazière, M. Validation of TANSO-FTS/GOSAT X_{CO_2} and X_{CH_4} glint mode retrievals using TCCON data from near-ocean sites. *Atmos. Meas. Tech.* **2016**, *9*, 1415–1430.
19. Eldering, A.; O'Dell, C.W.; Wennberg, P.O.; Crisp, D.; Gunson, M.R.; Viatte, C.; Avis, C.; Braverman, A.; Castano, R.; Chang, A.; et al. The Orbiting Carbon Observatory-2: First 18 months of science data products. *Atmos. Meas. Tech.* **2017**, *10*, 549–563.
20. Crisp, D.; Pollock, H.R.; Rosenberg, R.; Chapsky, L.; Lee, R.A.M.; Oyafuso, F.A.; Frankenberg, C.; O'Dell, C.W.; Bruegge, C.J.; Doran, G.B.; et al. The on-orbit performance of the Orbiting Carbon Observatory-2 (OCO-2) instrument and its radiometrically calibrated products. *Atmos. Meas. Tech.* **2017**, *10*, 59–81.
21. Zhao, C.L.; Tans, P.P. Estimating uncertainty of the WMO mole fraction scale for carbon dioxide in air. *J. Geophys. Res.* **2006**, *111*, doi:10.1029/2005JD006003.
22. Wunch, D.; Toon, G.C.; Wennberg, P.O.; Wofsy, S.C.; Stephens, B.B.; Fischer, M.L.; Uchino, O.; Abshire, J.B.; Bernath, P.; Biraud, S.C.; et al. Calibration of the total carbon column observing network using aircraft profile data. *Atmos. Meas. Tech.* **2010**, *3*, 1351–1362.
23. Deutscher, N.M.; Griffith, D.W.T.; Bryant, G.W.; Wennberg, P.O.; Toon, G.C.; Washenfelder, R.A.; Keppel-Aleks, G.; Wunch, D.; Yavin, Y.; Allen, N.T.; et al. Total column X_{CO_2} measurements at Darwin Australia: Site description and calibration against in situ aircraft profiles. *Atmos. Meas. Tech.* **2010**, *3*, 947–958.
24. Messerschmidt, J.; Geibel, M.C.; Blumenstock, T.; Chen, H.; Deutscher, N.M.; Engel, A.; Feist, D.G.; Gerbig, C.; Gisi, M.; Hase, F.; et al. Calibration of TCCON column-averaged CO_2: the first aircraft campaign over European TCCON sites. *Atmos. Meas. Tech.* **2011**, *11*, 10765–10777.
25. Mandrake, L.; O'Dell, C.W.; Wunch, D.; Wennberg, P.O.; Fisher, B.; Osterman, G.B.; Marchetti, Y.; Eldering, A. *Orbiting Carbon Observatory-2 (OCO-2) Warn Level, Bias Correction, and Lite File Product Description*; Technical Report; California Institute of Technology: Pasasdena, CA, USA, 2017.
26. Wunch, D.; Wennberg, P.O.; Osterman, G.; Fisher, B.; Naylor, B.; Roehl, C.M.; O'Dell, C.; Mandrake, L.; Viatte, C.; Kiel, M.; et al. Comparisons of the Orbiting Carbon Observatory-2 (OCO-2) X_{CO_2} measurements with TCCON. *Atmos. Meas. Tech.* **2017**, *10*, 2209–2238.
27. Fisher, J.A.; Murray, L.T.; Jones, D.B.A.; Deutscher, N.M. Improved method for linear carbon monoxide simulation and source attribution in atmospheric chemistry models illustrated using GEOS-Chem v9. *Geosci. Model Dev. Discuss.* **2017**, *10*, 4126–4144.
28. European Commission. Emission Database for Global Atmospheric Research (EDGAR); Technical Report; Joint Research Centre (JRC)/Netherlands Environmental Assessment Agency (PBL): The Netherlands, 2011. Available online: http://edgar.jrc.ec.europa.eu/ (accessed on 30 October 2017).
29. Li, M.; Zhang, Q.; Kurokawa, J.; Woo, J.H.; He, K.; Lu, Z.; Ohara, T.; Song, Y.; Streets, D.G.; Carmichael, G.R.; et al. MIX: A mosaic Asian anthropogenic emission inventory under the international collaboration framework of the MICS-Asia and HTAP. *Atmos. Chem. Phys.* **2017**, *17*, 935–963.

30. Vestreng, V.; Mareckova, K.; Kakareka, S.; Malchykhina, A.; Kukharchyk, T. *Inventory Review 2007; Emission Data Reported to LRTAP Convention and NEC Directive*; MSC-W Technical Report; UNFCCC: New York, NY, USA, 2007; Volume 1.
31. Van Donkelaar, A.; Martin, R.V.; Pasch, A.N.; Szykman, J.J.; Zhang, L.; Wang, Y.X.; Chen, D. Improving the accuracy of daily satellite-derived ground-level fine aerosol concentration estimates for North America. *Environ. Sci. Technol.* **2012**, *46*, 11971–11978.
32. EPA, U.S. Available online: http://www.epa.gov/ttnchie1/net/2005inventory.html (accessed on 27 November 2017).
33. Kuhns, H.; Knipping, E.M.; Vukovich, J.M. Development of a United States–Mexico emissions inventory for the Big Bend Regional Aerosol and Visibility Observational (BRAVO) Study. *J. Air Waste Manag. Assoc.* **2005**, *55*, 677–692.
34. Yevich, R.; Logan, J.A. An assessment of biofuel use and burning of agricultural waste in the developing world. *Glob. Biogeochem. Cycles* **2003**, *17*, doi:10.1029/2002GB001952.
35. Lee, C.; Martin, R.V.; van Donkelaar, A.; Lee, H.; Dickerson, R.R.; Hains, J.C.; Krotkov, N.; Richter, A.; Vinnikov, K.; Schwab, J.J. SO_2 emissions and lifetimes: Estimates from inverse modeling using in situ and global, space-based (SCIAMACHY and OMI) observations. *J. Geophys. Res. Atmos.* **2011**, *116*, doi:10.1029/2010JD014758.
36. Stettler, M.; Eastham, S.; Barrett, S. Air quality and public health impacts of UK airports. Part I: Emissions. *Atmos. Environ.* **2011**, *45*, 5415–5424.
37. Darmenov, A.; da Silva, A. *The Quick Fire Emissions Dataset (QFED)–Documentation of Versions 2.1, 2.2 and 2.4*; NASA Technical Report Series on Global Modeling and Data Assimilation, NASA TM-2013-104606; NASA: Washington, DC, USA, 2013; Volume 32, p. 183.
38. Guenther, A.B.; Jiang, X.; Heald, C.L.; Sakulyanontvittaya, T.; Duhl, T.; Emmons, L.K.; Wang, X. The Model of Emissions of Gases and Aerosols from Nature version 2.1 (MEGAN2.1): An extended and updated framework for modeling biogenic emissions. *Geosci. Model Dev.* **2012**, *5*, 1471–1492.
39. Stein, A.F.; Draxler, R.R.; Rolph, G.D.; Stunder, B.J.B.; Cohen, M.D.; Ngan, F. NOAA's HYSPLIT atmospheric transport and dispersion modeling system. *Bull. Am. Meteorol. Soc.* **2015**, *96*, 2059–2077.
40. Velazco, V.; Notholt, J.; Warneke, T.; Lawrence, M.; Bremer, H.; Drummond, J.; Schulz, A.; Krieg, J.; Schrems, O. Latitude and altitude variability of carbon monoxide in the Atlantic detected from ship-borne Fourier transform spectrometry model, and satellite data. *J. Geophys. Res.* **2005**, *110*, doi:10.1029/2004JD005351.
41. Ridder, T.; Gerbig, C.; Notholt, J.; Rex, M.; Schrems, O.; Warneke, T.; Zhang, L. Ship-borne FTIR measurements of CO and O_3 in the Western Pacific from 43°N to 35°S: An evaluation of the sources. *Atmos. Chem. Phys.* **2012**, *12*, 815–828.
42. O'Dell, C.W.; Eldering, A.; Crisp, D.; Fisher, B.; Gunson, M.; McDuffie, J.; Mandrake, L.; Smyth, M.; Wennberg, P.; Wunch, D. Recent Improvements in X_{CO_2} Measurements from OCO-2. In Proceedings of the 13th International Workshop on Greenhouse Gas Measurements from Space, Helsinki, Finland, 6–8 June 2017; p. 54.
43. Kobayashi, S.; Ota, Y.; Harada, Y.; Ebita, A.; Moriya, M.; Onoda, H.; Onogi, K.; Kamahori, H.; Kobayashi, C.; EndoO, H.; et al. The JRA-55 Reanalysis: General specifications and basic characteristics. *J. Meteorol. Soc. Jpn. Ser. II* **2015**, *93*, 5–48.
44. Uchino, O.; Sakai, T.; Izumi, T.; Nagai, T.; Morino, I.; Yamazaki, A.; Deushi, M.; Yumimoto, K.; Maki, T.; Tanaka, T.Y.; et al. LiDAR detection of high concentrations of ozone and aerosol transported from northeastern Asia over Saga Japan. *Atmos. Chem. Phys.* **2017**, *17*, 1865–1879.
45. Huang, R.J.; Zhang, Y.; Bozzetti, C.; Ho, K.F.; Cao, J.J.; Han, Y.; Daellenbach, K.R.; Slowik, J.G.; Platt, S.M.; Canonaco, F.; et al. High secondary aerosol contribution to particulate pollution during haze events in China. *Nature* **2014**, *514*, 218–222.
46. Reid, J.S.; Xian, P.; Hyer, E.J.; Flatau, M.K.; Ramirez, E.M.; Turk, F.J.; Sampson, C.R.; Zhang, C.; Fukada, E.M.; Maloney, E.D. Multi-scale meteorological conceptual analysis of observed active fire hotspot activity and smoke optical depth in the Maritime Continent. *Atmos. Chem. Phys.* **2012**, *12*, 2117–2147.
47. Lasco, R.D.; Lales, J.S.; Arnuevo, M.; Guillermo, I.Q.; de Jesus, A.C.; Medrano, R.; Bajar, O.F.; Mendoza, C.V. Carbon dioxide (CO_2) storage and sequestration of land cover in the Leyte Geothermal Reservation. *Renew. Energy* **2002**, *25*, 307–315.

48. Suto, H.; Yajima, Y.; Nakajima, M. Airborne-Based Demonstration of Intelligent Pointing Onboard GOSAT-2. In Proceedings of the 13th International Workshop on Greenhouse Gas Measurements from Space, Helsinki, Finland, 6–8 June 2017; p. 87.
49. Deutscher, N.M.; Sherlock, V.; Fletcher, S.E.M.; Griffith, D.W.T.; Notholt, J.; Macatangay, R.; Connor, B.J.; Robinson, J.; Shiona, H.; Velazco, V.A.; et al. Drivers of column-average CO_2 variability at Southern Hemispheric Total Carbon Column Observing Network sites. *Atmos. Chem. Phys.* **2014**, *14*, 9883–9901.
50. Liu, H. Transport pathways for Asian pollution outflow over the Pacific: Interannual and seasonal variations. *J. Geophys. Res.* **2003**, *108*, doi:10.1029/2002JD003102.
51. Bohren, C.F.; Huffman, D.R. *Absorption and Scattering of Light by Small Particles*; Wiley-VCH: Weinheim, Germany, 1983.
52. Sakai, T.; Shibata, T.; Iwasaka, Y.; Nagai, T.; Nakazato, M.; Matsumura, T.; Ichiki, A.; Kim, Y.S.; Tamura, K.; Troshkin, D.; et al. Case study of Raman LiDAR measurements of Asian dust events in 2000 and 2001 at Nagoya and Tsukuba Japan. *Atmos. Environ.* **2002**, *36*, 5479–5489.
53. Velazco, V. LIDAR Studies of Water Vapor and Aerosols in the Boundary Layer in the Southern Hemisphere and in the Arctic. Master's Thesis, University of Bremen, Bremen, Germany, 2002.
54. Heese, B.; Baars, H.; Bohlmann, S.; Althausen, D.; Deng, R. Continuous vertical aerosol profiling with a multi-wavelength Raman polarization LiDAR over the Pearl River Delta China. *Atmos. Chem. Phys.* **2017**, *17*, 6679–6691.
55. Belikov, D.A.; Maksyutov, S.; Ganshin, A.; Zhuravlev, R.; Deutscher, N.M.; Wunch, D.; Feist, D.G.; Morino, I.; Parker, R.J.; Strong, K.; et al. Study of the footprints of short-term variation in X_{CO_2} observed by TCCON sites using NIES and FLEXPART atmospheric transport models. *Atmos. Chem. Phys.* **2017**, *17*, 143–157.